The Journal of Chemical Physics

RESEARCH ARTICLE | NOVEMBER 03 2025

Self-assembly of inverted phases in AB/CD diblock copolymer blends

Special Collection: Self-Assembly: From Blueprints to Breakthroughs

Yuhui Yi ; Jiayu Xie ; Jiajia Zhou ; An-Chang Shi

J. Chem. Phys. 163, 174901 (2025)
https://doi.org/10.1063/5.0299462

The Journal of Chemical Physics | ARTICLE | pubs.aip.org/aip/jcp

Self-assembly of inverted phases in AB/CD diblock copolymer blends

Cite as: J. Chem. Phys. 163, 174901 (2025); doi: 10.1063/5.0299462
Submitted: 27 August 2025 • Accepted: 12 October 2025 •
Published Online: 3 November 2025

Yuhui Yi,[1] Jiayu Xie,[1] Jiajia Zhou,[2,3] and An-Chang Shi[1,a)]

AFFILIATIONS

[1] Department of Physics and Astronomy, McMaster University, Hamilton, Ontario L8S 4M1, Canada
[2] South China Advanced Institute for Soft Matter Science and Technology, School of Emergent Soft Matter, South China University of Technology, Guangzhou 510640, China
[3] Guangdong Provincial Key Laboratory of Functional and Intelligent Hybrid Materials and Devices, South China University of Technology, Guangzhou 510640, China

Note: This paper is part of the Special Topic, Self-Assembly: From Blueprints to Breakthroughs.
[a)] **Author to whom correspondence should be addressed:** shi@mcmaster.ca

ABSTRACT

Conventional ordered phases of block copolymers are nanoscopic structures with discrete domains (spheres or cylinders) composed of the minority blocks embedded in a continuous matrix composed of the majority blocks. Inverted phases of block copolymers refer to the novel ordered structures with discrete domains composed of the majority blocks. In this work, the formation and relative stability of various inverted phases in AB/CD diblock copolymer blends are studied using self-consistent field theory. The results reveal that the ratio of the block copolymer lengths and the copolymer concentration play a crucial role in stabilizing the inverted structures, and the relative stability of various inverted phases depends sensitively on the interaction strengths. The spatial distribution of the different blocks is used to elucidate mechanisms for the formation of inverted phases. The findings provide insights into the formation of inverted phases and suggest design strategies for functional nanostructures with potential applications in nanolithography and photonic crystals.

I. INTRODUCTION

Block copolymers (BCPs) have attracted sustained attention due to their ability to form ordered nanoscopic structures, which are obtained by the packing of self-assembled polymeric domains, including lamellae, cylinders, and spheres.[1] For linear AB diblock copolymers (DBCPs), the simplest BCPs composed of A and B homopolymers covalently linked at their ends, the ordered phases include hexagonally close-packed spheres (HCP), body-centered cubic spheres (BCC), hexagonally packed cylinders (HEX), double gyroid networks (DG), Fddd networks (O^{70}), and lamellae (LAM).[2] Furthermore, complex spherical packing phases, namely the Frank–Kasper (FK) σ and A15 phases, can be formed by linear AB diblock copolymers with large conformational asymmetry.[3,4] The formation of these nanostructures is driven by a delicate balance between minimizing the unfavorable inter-block contact and maximizing the conformational entropy.[2,5] It is commonly observed that the conventional ordered structures of BCPs, where the minority blocks form the dispersed domains and the majority blocks constitute the continuous matrix, are the dominant equilibrium phases. The phase behavior of block copolymers is primarily controlled by the block–block interactions, quantified by the product χN, where χ is the Flory–Huggins interaction parameter between the A and B blocks, and N is the degree of polymerization of the block copolymers.[2] For conformationally symmetric AB DBCPs at $\chi N \gg (\chi N)_c \approx 10.5$, phase transitions follow the sequence of disordered (Dis) → HCP → BCC → HEX → DG → LAM when the volume fraction of the A or B blocks is increased from 0 to 0.5.[1,2,6]

The formation of conventional ordered phases is in accordance with the intuitively obvious expectation that the interfaces tend to curve toward the component with a smaller volume fraction.[6] On the other hand, the formation of inverted phases of BCPs, where the components with larger volume fractions form discrete domains, violates the expected interfacial curvature; thus, such phases are commonly metastable or even unstable. The possible emergence of inverted morphologies as equilibrium phases must originate from mechanisms favoring interfaces with smaller curvature.[7] Moreover, inverted phases are of significant interest, both for elucidating the fundamental principles of self-assembly and for their potential applications in materials science, including nanolithography,[8] optical materials,[9] and membranes.[10] The unique physical and chemical properties of inverted phases expand the functional capabilities of BCPs, enabling the development of materials with tailored properties. From a fundamental perspective, investigating inverted phases could shed light on the understanding of self-assembly processes in soft matter physics and provide new insights into the thermodynamic behavior of polymeric systems.

Extensive experimental and theoretical studies have shown that inverted phases are metastable or unstable in linear AB diblock copolymers;[2,6] therefore, more complex BCP systems, such as multiblock copolymers, nonlinear block copolymers, and block copolymer blends, are required to stabilize these unconventional ordered phases. The term "inverted phase" was mentioned by Pico and Williams in their study of ABA triblock copolymers in 1977,[11,12] where the formation of an inverted HEX phase was associated with conditions where entropic contributions outweigh the enthalpic penalties of larger interfacial areas. More recently, inverted HEX phases have been observed in nonlinear star block copolymers.[13,14] Furthermore, Seo *et al.* reported the observation of an inverted DG phase in PS-(PS-b-P2VP)$_3$ miktoarm star copolymers.[15] It is noted that inverted phases could be induced via non-equilibrium pathways, where variations in solvent concentration, temperature, or evaporation rate kinetically promote the formation of such unconventional structures. For example, Zhang *et al.* reported an inverted HEX phase in poly(styrene-b-butadiene-b-styrene) triblock copolymers that is regulated by the solvent evaporation rate.[16]

Compared with polymer melts composed of neat block copolymers, polymer blends containing multiple types of BCPs offer the opportunity to regulate their phase behavior via differential distributions of the different components,[17] providing an effective and efficient platform to obtain inverted phases. An early example of this strategy is the experimental observation of an inverted HEX phase in binary blends of polystyrene–*block*–polyisoprene with high and low molecular weights by Yamaguchi *et al.*[18] Furthermore, the introduction of hydrogen bonding to the blend system could lead to the formation of more diverse inverted structures, such as the inverted HEX phase[19] and the inverted tetragonally-packed cylindrical (TET) phase.[20] One interesting observation from these studies is that the formation of inverted phases requires a small ratio of molecular weights of the two BCPs (≤ 0.2). Going beyond linear BCPs, Li *et al.* used self-consistent field theory (SCFT) to predict that various inverted cylindrical and spherical phases can be formed in binary blends composed of A(AB)$_3$ miktoarm star copolymers and AC diblock copolymers.[21] Inspired by the success of binary blends composed of AB and AB diblock copolymers,[17] it is natural to inquire whether extending the blends from AB/AB to AB/CD diblock copolymers could promote the formation and stability of inverted phases.

In the absence of attractive interactions between the AB and CD DBCPs, the phase behavior of AB/CD blends is dominated by macroscopic phase separation, resulting in coexisting AB-rich and CD-rich phases.[22] An effective avenue to inhibit macroscopic phase separation is to introduce attractive interactions, such as hydrogen bonding or π–π stacking, between the two different BCPs. It has been shown that introducing attraction between the B and D blocks greatly enlarges the one-phase region for AB/CD blends, providing opportunities to form various ordered phases that are not available in the corresponding neat DBCP melts.[22–24] The phase behavior of AB/CD diblock copolymer blends is controlled by a large number of parameters, including the molecular weights and composition of the two DBCPs, the volume fractions of the different blocks, and the various interaction parameters between the blocks. Varying these parameters provides opportunities to stabilize various novel morphologies. As an example, Xie *et al.*[22] used SCFT to examine the emergence of various spherical packing phases in AB/CD DBCP blends and demonstrated the formation of ordered phases composed of A + C mixed spheres or binary A/C-separated spheres. The formation of various spherical packing phases in similar AB/B′C binary blends has been studied by Dorfman and co-workers.[23,24]

In the current study, we focus on the formation of inverted phases from binary blends of linear diblock copolymers. Specifically, we use SCFT to investigate the emergence and relative stability of various inverted phases in binary blends composed of linear AB and CD diblock copolymers, emphasizing the influence of copolymer composition and volume fractions on their phase behavior. The conditions stabilizing the inverted morphologies are identified, thereby providing insights into the formation principles of these novel phases and guidance for the design of advanced functional materials.

The rest of the paper is organized as follows. Section II describes the model system and the self-consistent field theory for the binary blends. Section III presents the results of the theoretical study in terms of a set of phase diagrams, segment distributions, and related discussions, demonstrating the formation of various inverted phases. Section IV gives a brief summary and possible future extension of the study.

II. BLOCK COPOLYMER MODEL AND THEORETICAL FRAMEWORK

We consider a model of binary blends composed of two, AB and CD, diblock copolymers, shown schematically in Fig. 1. The interaction parameters between the different blocks are chosen to prevent macroscopic phase separation and to enhance the formation of ordered phases composed of two separated AB-rich and BD-rich partitions. The phase behavior of AB/CD blends is governed by a large number of parameters, including two molecular weights, two volume fractions of the blocks, six interaction parameters, and the copolymer concentrations. Exploring the phase behavior of the blends within the whole parameter space presents an insurmountable task. In the current study, we focus on the formation of inverted

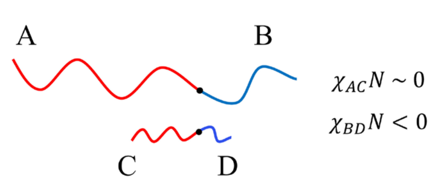

FIG. 1. Schematics of AB and CD diblock copolymers. The A and C blocks are miscible with $\chi_{AC}N \sim 0$, whereas the B and D blocks attract each other via secondary interactions described by a negative $\chi_{BD}N < 0$.

phases in a restricted parameter space. Specifically, the model is designed such that the B and D blocks are attractive to each other, whereas the A and C blocks are miscible, which could be achieved by choosing $\chi_{BD} < 0$[25] and $\chi_{AC} \sim 0$. Furthermore, the A and C blocks are assumed to be the majority blocks with their combined volume fraction $f_{AC} > 0.5$, such that the inverted phases of the AB/CD blends are formed from the packing of domains composed of A and C blocks embedded in a continuous matrix composed of B and D blocks.

Specifically, the model system is comprised of n_1 AB DBCPs and n_2 CD DBCPs contained in a volume V. All the polymeric species are modeled as Gaussian chains. The degrees of polymerization of the copolymers are $N_1 = N_A + N_B$ and $N_2 = N_C + N_D$ for the AB and CD DBCPs, respectively. $N = N_1$ is chosen as the reference degree of polymerization, and the chain length of the CD DBCPs is quantified by the chain length ratio $\gamma = N_2/N_1$. The compositions of the two DBCPs are specified by the volume fraction of the A and C blocks, $f_1 = f_A = N_A/N_1$ and $f_2 = f_C = N_C/N_2$, respectively. All the segments are assumed to have the same volume $v_0 = \rho_0^{-1}$ and the incompressibility condition requires $(n_1 N + n_2 \gamma N)/\rho_0 V = 1$. The average concentrations of the AB and CD DBCPs are given by, $\phi_1 = (n_1 N)/(\rho_0 V)$ and $\phi_2 = (n_2 \gamma N)/(\rho_0 V) = 1 - \phi_1$, respectively. An important parameter is the combined volume fraction of A and C blocks given by $f_{AC} = f_1(1-\phi_2) + f_2\phi_2$.

The phase behavior of block copolymer blends is most conveniently studied by using the self-consistent field theory formulated in the grand canonical ensemble.[26,27] A brief account of the theory is given below, while details of the SCFT formulation are found in the literature.[22] In the grand canonical ensemble, the chemical potentials, μ_1 and μ_2, of the AB and CD DBCPs are the thermodynamic control parameters. Due to the incompressibility condition, these two chemical potentials are not independent. In the current study, μ_1 is regarded as the reference such that $\mu_1 = 0$ and $\mu_2 = \mu$. Within the SCFT, the grand potential density of the system is given by[22]

$$\begin{aligned}\frac{N\Phi}{\rho_0 V k_B T} = -Q_1 - zQ_2 - \frac{1}{V}\int d\vec{r}\Bigg[\sum_{\alpha}\omega_\alpha(\vec{r})\phi_\alpha(\vec{r}) \\ - \frac{1}{2}\sum_{\alpha,\ \beta\ (\neq\alpha)}\chi_{\alpha\beta}N\phi_\alpha(\vec{r})\phi_\beta(\vec{r}) \\ + \eta(\vec{r})\left(1 - \sum_{\alpha}\phi_\alpha(\vec{r})\right)\Bigg]. \end{aligned} \tag{1}$$

Here, $\phi_\alpha(\vec{r})$ and $\omega_\alpha(\vec{r})$ (α = A, B, C, or D) are the density and conjugate fields describing the spatial distribution of the polymeric species and the local chemical potentials, respectively, $\chi_{\alpha\beta}$ refers to the Flory–Huggins interaction parameter between α and β monomers, and $\eta(\vec{r})$ is a Lagrange field introduced to enforce the incompressibility condition, $\sum_\alpha \phi_\alpha(\vec{r}) = 1$. The chemical potential μ is specified in terms of the fugacity $z = e^{\mu/k_B T}$. The quantities Q_1 and Q_2 are the single-chain partition functions of the DBCPs that will be specified below.

The central task of the SCFT is to find minima of the grand potential or the free energy, which represent possible equilibrium phases of the system. Minimizing the grand potential with respect to the density field $\phi_\alpha(\vec{r})$, conjugate field $\omega_\alpha(\vec{r})$, and the Lagrange field $\eta(\vec{r})$ leads to a set of SCFT equations:

$$\begin{cases}\omega_\alpha(\vec{r}) = \sum\limits_{\beta(\neq\alpha)}\chi_{\alpha\beta}N\phi_\beta(\vec{r}) + \eta(\vec{r}),\\ \phi_A(\vec{r}) = \int_0^{f_1} ds q_1(s,\vec{r})q_1^\dagger(s,\vec{r}),\\ \phi_B(\vec{r}) = \int_{f_1}^{1} ds q_1(s,\vec{r})q_1^\dagger(s,\vec{r}),\\ \phi_C(\vec{r}) = z\int_0^{\gamma f_2} ds q_2(s,\vec{r})q_2^\dagger(s,\vec{r}),\\ \phi_D(\vec{r}) = z\int_{\gamma f_2}^{\gamma} ds q_2(s,\vec{r})q_2^\dagger(s,\vec{r}),\\ \sum\limits_\alpha \phi_\alpha(\vec{r}) = 1,\end{cases} \tag{2}$$

where $q(s,\vec{r})$ and $q^\dagger(s,\vec{r})$ are the forward and backward propagators, respectively. These propagators are obtained by solving the following modified diffusion equations:

$$\begin{cases}\frac{\partial}{\partial s}q_1(s,\vec{r}) = \frac{Nb_1^2}{6}\nabla^2 q_1(s,\vec{r}) - \omega_1(\vec{r})q_1(s,\vec{r}),\\ -\frac{\partial}{\partial s}q_1^\dagger(s,\vec{r}) = \frac{Nb_1^2}{6}\nabla^2 q_1^\dagger(s,\vec{r}) - \omega_1(\vec{r})q_1^\dagger(s,\vec{r}),\\ \frac{\partial}{\partial s}q_2(s,\vec{r}) = \frac{Nb_2^2}{6}\nabla^2 q_2(s,\vec{r}) - \omega_2(\vec{r})q_2(s,\vec{r}),\\ -\frac{\partial}{\partial s}q_2^\dagger(s,\vec{r}) = \frac{Nb_2^2}{6}\nabla^2 q_2^\dagger(s,\vec{r}) - \omega_2(\vec{r})q_2^\dagger(s,\vec{r}).\end{cases} \tag{3}$$

Here, b_α is the Kuhn length of the α chain. The counter length variable $s \in [0,1]$ for AB DBCPs and $s \in [0,\gamma]$ for CD DBCPs, respectively. Moreover, $\omega_1(\vec{r}) = \omega_A(\vec{r})$ and $b_1 = b_A$ if $s \in [0, f_1]$, while $\omega_1(\vec{r}) = \omega_B(\vec{r})$ and $b_1 = b_B$ if $s \in [f_1, 1]$ for AB DBCPs. Similarly, $\omega_2(\vec{r}) = \omega_C(\vec{r})$ and $b_2 = b_C$ if $s \in [0, \gamma f_2]$, while $\omega_1(\vec{r}) = \omega_B(\vec{r})$ and $b_2 = b_D$ if $s \in [\gamma f_2, \gamma]$ for CD DBCPs. The initial conditions of the propagators are specified by $q_1(0,\vec{r}) = q_2(0,\vec{r}) = q_1^\dagger(1,\vec{r}) = q_2^\dagger(\gamma,\vec{r}) = 1$. Finally, the single-chain partition functions, Q_1 and Q_2, are given by the integrals of the propagators:

$$\begin{cases}Q_1 = \frac{1}{V}\int d\vec{r}\ q_1(1,\vec{r}),\\ Q_2 = \frac{1}{V}\int d\vec{r}\ q_2(\gamma,\vec{r}).\end{cases} \tag{4}$$

The average concentrations of the AB and CD DBCPs are given by the single-chain partition functions:

$$\begin{cases}\phi_1 = Q_1,\\ \phi_2 = 1 - \phi_1.\end{cases} \tag{5}$$

The SCFT equations [Eq. (2)] form a set of nonlinear and nonlocal equations. Analytic solutions of these equations are only possible for the homogeneous (disordered) phase. On the other hand, accurate and efficient algorithms have been developed for solving the SCFT equations numerically.[28] Numerical solutions of the SCFT equations are obtained most conveniently by iterations, which depend on the initial conditions corresponding to candidate phases of the system. Ten ordered structures including lamellae (L), two types of cylinders (HEX and TET), five types of spheres (BCC, FCC, HCP, A15, and σ), and two types of networks (DG and O^{70}), together with their inverted version, are used in the current study. Schematics of these candidate phases are shown in Fig. 2. It is noted that the set of structures shown in Fig. 2 does not exhaust all

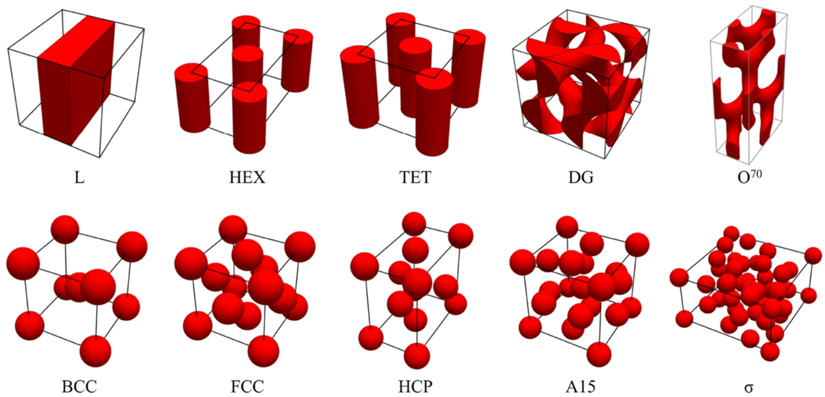

FIG. 2. Schematics of candidate phases used in the current study.

possibilities of the ordered candidates. Rather, we follow the common practice[29] by considering as many candidate phases as possible. These structures are usually observed in both theoretical calculations and experiments in block copolymers and binary block copolymer blends.

Starting from a candidate structure with a specified crystalline symmetry, an accurate numerical solution of the SCFT equations corresponding to a local minimum of the free energy landscape could be obtained via iteration. For a given set of the conjugate fields $\omega_\alpha(\vec{r})$, the propagators are obtained by solving the modified

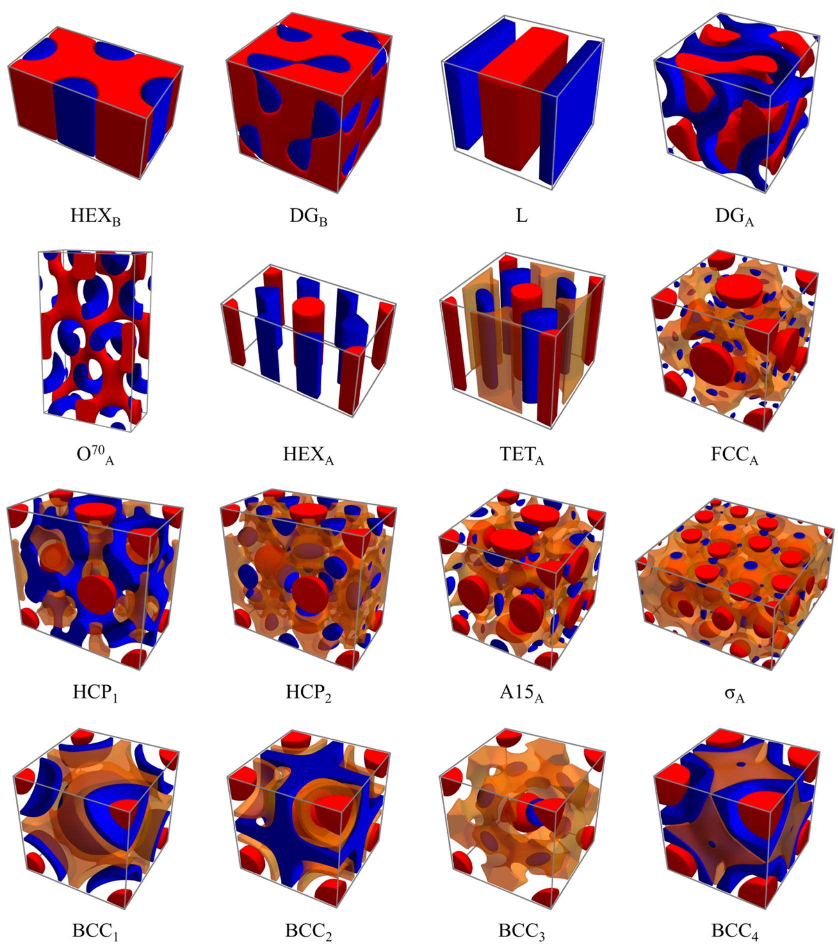

FIG. 3. Schematics of typical solutions of the SCFT equations corresponding to various ordered phases. The A and B + D domains are shown in red and blue, respectively. For the inverted phase, when applicable, the C domains are also shown in semi-transparent orange.

diffusion equations [Eq. (3)] using the pseudo-spectral method.[30,31] We also apply the variable-cell Anderson mixing method[32,33] to simultaneously speed up the convergence of solutions to Eq. (2) and to optimize the unit-cell parameters. For the binary blends composed of AB and CD DBCPs, this procedure leads to many solutions of the SCFT equations, corresponding to possible equilibrium phases of the system. Figure 3 shows typical SCFT solutions corresponding to various ordered phases. The phase diagrams of the system and the relative stability of the different phases are obtained by comparing the grand potential densities of the different solutions corresponding to the candidate phases.

III. RESULTS AND DISCUSSION

A. Ordered phases predicted by SCFT

The model system of binary AB/CD DBCP blends contains a large number of parameters. In the current study, the molecular parameters are chosen such that the AB and CD DBCPs imitate the experimentally studied polystyrene-*block*-poly(4-vinylpyridine) (PS-b-P4VP) and polystyrene-*block*-poly(4-hydroxystyrene) (PS-b-PHS), respectively, so that the theoretical results can be compared with experiments. The Flory–Huggins interaction parameters between these polymeric species have been estimated based on experiments as $\chi_{\mathrm{PS-P4VP}} \approx 0.3$, $\chi_{\mathrm{PS-PHS}} \approx 0.6$, and $\chi_{\mathrm{P4VP-PHS}} \approx -0.17$,[34] reflecting strong repulsion between PS and PHS, moderate incompatibility between PS and P4VP, and weak attraction between P4VP and PHS. These interaction parameters serve as the basis for modeling scenarios with asymmetric interactions. Choosing the A and C blocks as the PS block with $\chi_{\mathrm{AC}}N \sim 0$ results in a simplified but representative case for blends with miscible A and C blocks. We further set a chain-length ratio $\gamma < 1$ to capture the influence of molecular asymmetry. In all the calculations, the statistical segment length is set to be the same $b_\alpha = b$; thus, we consider conformationally symmetric systems in the current study. The volume fractions (f_{A} and f_{C}) of the A and C blocks are assumed to be larger than 0.5 so that the B and D blocks form the minority blocks of the system.

The choice of $\chi_{\mathrm{AC}}N = 0$ and $\chi_{\mathrm{AX}}N = \chi_{\mathrm{CX}}N$ (with X = B or D) implies that the A and C blocks are chemically identical; thus, the AB/CD blends become AB/A′D blends. Therefore, the results presented for our choice of the interaction parameters could be regarded as those of AB/A′D blends with attractive B/D interactions. However, these results are qualitatively valid for cases where the A and C blocks are chemically different but miscible ($\chi_{\mathrm{AC}}N \ll 1$). It is expected that increasing the A/C repulsion will modify the phase behavior of the AB/CD blends, eventually leading to complete separation and A and C domains. Exploring the phase behavior of binary blends of AB and CD DBCPs when $\chi_{\mathrm{AC}}N$ is varied from a very small value to a larger one is an interesting topic that will be left for a future study.

As shown in Fig. 3, various ordered phases can be formed from the co-assembly of the AB and CD DBCPs. In this work, regions with $\phi_\alpha > 0.5$ within a structure are defined as α-rich domains, where α denotes A, B, C, D, or any combination thereof (e.g., $\phi_{\mathrm{BD}} = \phi_{\mathrm{B}} + \phi_{\mathrm{D}}$). The naming convention of these ordered phases is that the subscript B or D denotes conventional phases with domains composed of the minority blocks (e.g., $\mathrm{HEX_B}$, where the minority B blocks form the cylindrical domains); the subscript A denotes inverted phases (e.g., $\mathrm{HEX_A}$, where the majority A blocks form the cylindrical domains); and numerical subscripts indicate topological variation of B and D domains within a given symmetry of the structure. These topological variations originate from the fact that in different structures, the C blocks exhibit different degrees of miscibility with the A blocks, and the mixed B and D blocks could form either an interconnected BD-rich network or discrete BD-rich domains.

Several HCP- and BCC-based structures featuring different morphologies of the BD-rich domains could be identified. Specifically, two different $\mathrm{HCP_A}$ phases, labeled as $\mathrm{HCP_1}$ and $\mathrm{HCP_2}$, are observed. In $\mathrm{HCP_1}$, the mixed BD blocks form a continuous skeleton, whereas in $\mathrm{HCP_2}$ they form discrete pie-shaped domains. Furthermore, four distinct $\mathrm{BCC_A}$ phases are identified: $\mathrm{BCC_1}$ has well-defined BD-rich spherical shells; $\mathrm{BCC_2}$ forms a continuous BD-rich network that is enriched at the square faces but depleted from the hexagonal faces of the BCC Wigner–Seitz cell (WSC); $\mathrm{BCC_3}$ contains discrete pie-shaped BD-rich domains on the hexagonal faces of the WSC; and $\mathrm{BCC_4}$ shows a continuous BD-rich network obtained by connecting the spherical shells in $\mathrm{BCC_1}$ through the hexagonal faces of the WSC. The different HCP- and BCC-based structures show free energy curves that are discontinuous from each other, and thus they are related by first-order phase transitions. In the current work, the BD-rich domains are consistently discontinuous in $\mathrm{A15_A}$, σ_{A}, and $\mathrm{FCC_A}$, while in $\mathrm{O^{70}_A}$, they form helices. The structures of these spherical phases and the $\mathrm{O^{70}}$ phase are shown in Fig. 3. Among all inverted phases emerged in our calculations, C-rich domains appear consistently only in the $\mathrm{TET_A}$ and spherical phases, while they are absent in all other structures. The C-rich domains in these phases are depicted in Fig. 3 as semi-transparent orange regions. Notably, for the various HCP- and BCC-based phases, the differences in their BD distributions are accompanied by distinct morphologies of the C-rich domains. It is noted that, although the three-dimensional density profiles shown in Fig. 3 provide a quantitative description of the different ordered structures, it is a challenge to define a single order parameter to describe the differences of these structures.

B. Emergence of inverted phases

As a starting point, we examine the phase behavior of an AB/CD blend with the following parameters: $\chi_{\mathrm{AB}}N = \chi_{\mathrm{BC}}N = 30$, $\chi_{\mathrm{AC}}N = 0$, $\chi_{\mathrm{AD}}N = \chi_{\mathrm{CD}}N = 60$, $f_1 = 0.75$, $f_2 = 0.62$, and $\gamma = 0.16$. This set of parameters is chosen such that the equilibrium phase of the AB DBCPs is hexagonally packed cylinders formed by the B blocks ($\mathrm{HEX_B}$), and the equilibrium phase of the shorter CD diblock copolymers is the disordered phase. The interaction parameter between the B and D blocks, $\chi_{\mathrm{BD}}N$, is varied from 0 to −24, to highlight the effect of B/D attraction on the formation of various ordered phases. The binary mixture of these two AB and CD DBCPs provides an interesting case to explore the order–order phase transitions induced by adding shorter DBCPs.

The phase diagram of the system is constructed by comparing the free energy density of different candidate phases. Figure 4(a) shows the grand potential densities of several representative ordered phases as a function of the fugacity, while Fig. 4(b) presents the corresponding free energy difference between the ordered phases and lamellae on the left, and between the ordered phases and the disordered phases on the right. These plots are for the case with

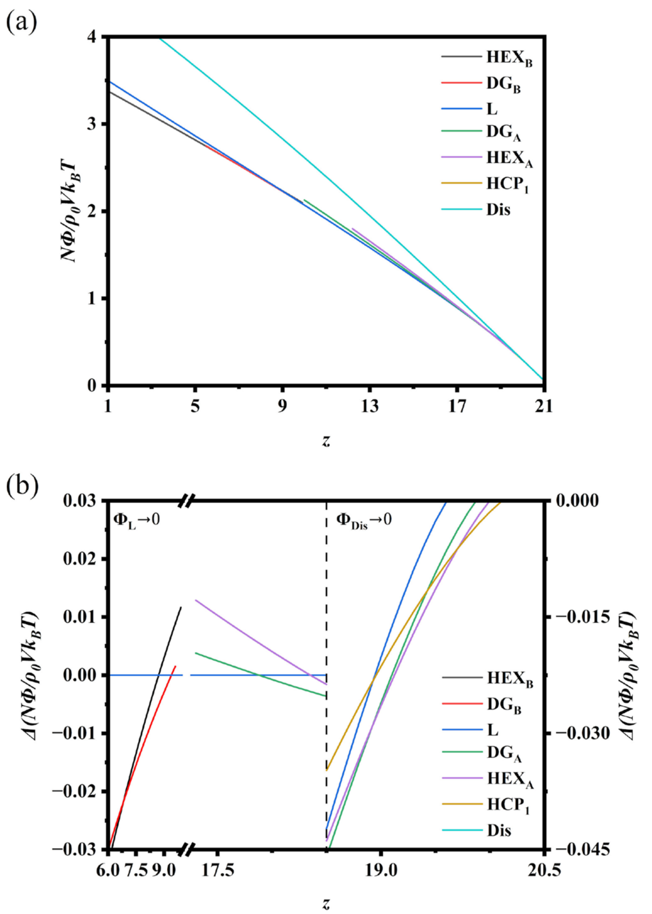

FIG. 4. Free energy plots of several representative phases of AB/CD blends with $\chi_{AB}N = 30$, $\chi_{AD}N = 60$, $\chi_{BC}N = 30$, $\chi_{CD}N = 60$, $\chi_{BD}N = 0$, $f_1 = 0.75$, $f_2 = 0.62$, and $\gamma = 0.16$: (a) grand potential density as a function of fugacity z and (b) relative grand potential density of the ordered phases with respect to the L phase in the fugacity range $z \in (6, 18.5)$, and with respect to the Dis phase in the range $z \in (18.5, 20.5)$.

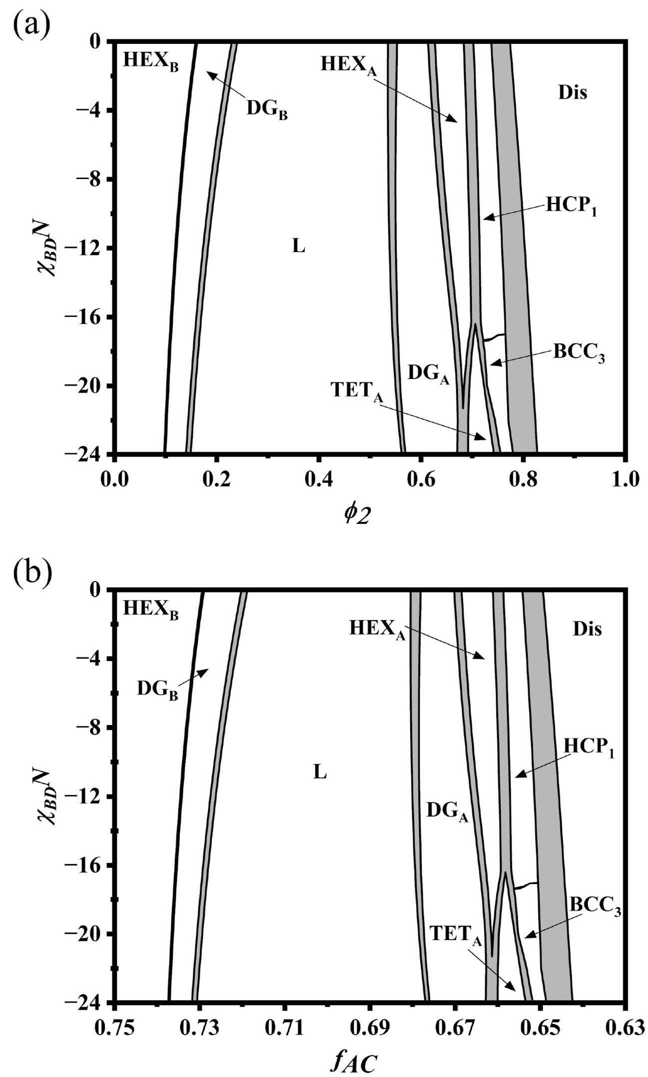

FIG. 5. Phase diagram and morphologies of AB/CD DBCP blends with $\chi_{AB}N = \chi_{BC}N = 30$, $\chi_{AC}N = 0$, $\chi_{AD}N = 60 = \chi_{CD}N = 60$, $f_1 = 0.75$, $f_2 = 0.62$, and $\gamma = 0.16$: (a) phase diagram in the $\chi_{BD}N - \phi_2$ plane; (b) phase diagram in the $\chi_{BD}N - f_{AC}$ plane.

$\chi_{BD}N = 0$, highlighting the order-to-order transitions induced by the addition of the shorter CD DBCPs. On this plot, each crossover of two free energy curves corresponds to a first-order phase transition between the two different ordered structures. The free energy plot reveals that, as the fugacity increases, the equilibrium phase evolves from HEX$_B$ to DG$_B$, L, DG$_A$, HEX$_A$, HCP$_1$, and finally to the disordered state. This phase transition sequence reflects the progressive shift from conventional B-rich cylindrical structures to inverted phases composed of A domains as the concentration of CD DBCPs increases. These trends will later be generalized and compared across different values of $\chi_{BD}N$. It is noted that this particular blend does not exhibit macroscopic phase separation because the CD DBCPs with $\gamma = 0.16$ are much shorter than the AB DBCP; thus, their translational entropy dominates the phase behavior.

Information about the phase behavior of the AB/CD blends is presented in two equivalent phase diagrams in the $\chi_{BD}N - \phi_2$ [Fig. 5(a)] and $\chi_{BD}N - f_{AC}$ [Fig. 5(b)] planes, highlighting the effect of adding the shorter CD DBCPs (ϕ_2) and the overall volume fraction of the A and C blocks (f_{AC}). The one-phase and two-phase coexistence regions in the phase diagrams are indicated in white and gray, respectively. The phase diagram shown in Fig. 5 reveals that the addition of CD DBCPs induces phase transitions following three sequences depending on the B/D attraction: (1) HEX$_B$ → DG$_B$ → L → DG$_A$ → HEX$_A$ → HCP$_1$ → Dis for $-16 < \chi_{BD}N \le 0$, (2) HEX$_B$ → DG$_B$ → L → DG$_A$ → HEX$_A$ → TET$_A$ → BCC$_3$ → Dis for $-20 < \chi_{BD}N < -16$, and (3) HEX$_B$ → DG$_B$ → L → DG$_A$ → TET$_A$ → BCC$_3$ → Dis for $\chi_{BD}N < -20$. Three of these ordered phases, DG$_A$, HEX$_A$, and TET$_A$, are inverted phases where the discrete domains are composed of A and C blocks with volume fractions $f_{AC} > 0.65$. The morphologies of the equilibrium phases are shown

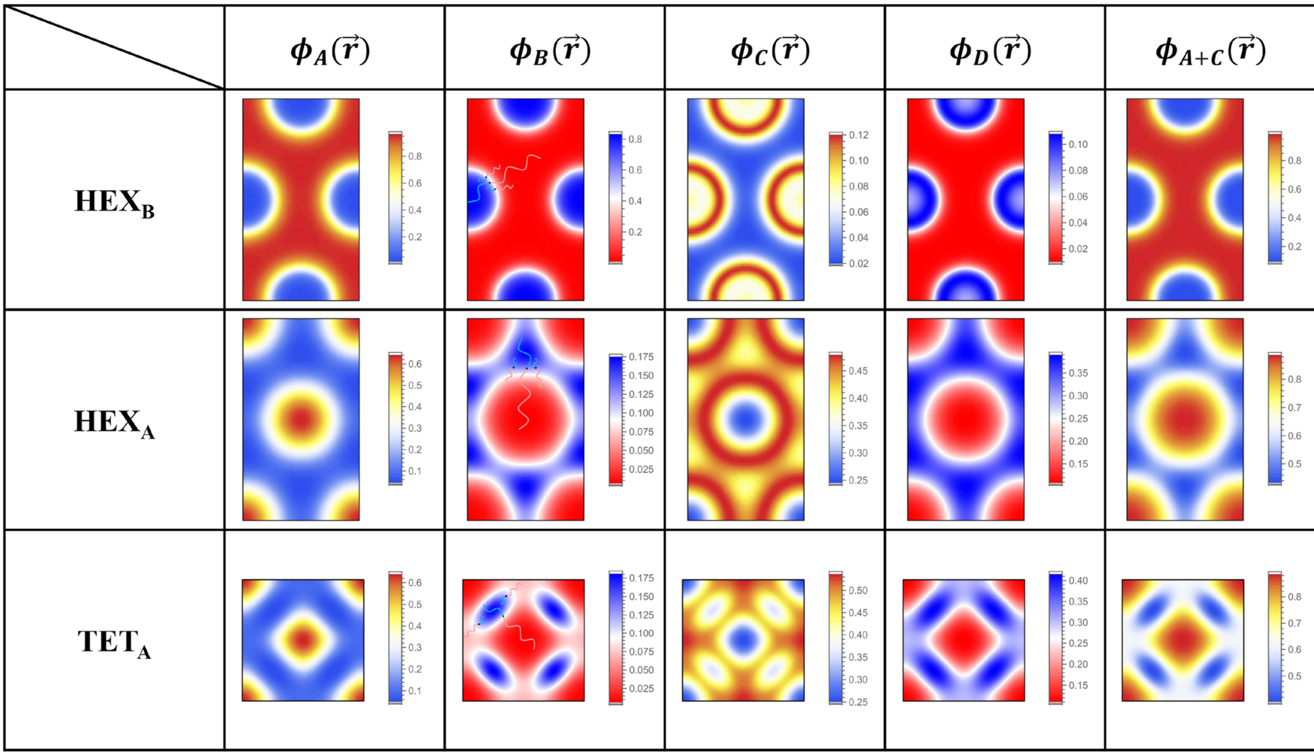

FIG. 6. Spatial distributions of segment densities for HEX_B, HEX_A, and TET_A. Each column displays the normalized density profiles of A, B, C, D, and A + C (from left to right), with a schematic representation of the polymer chains included in the B-component panel. The parameters used are $\chi_{AB}N = \chi_{BC}N = 30$, $\chi_{AC}N = 0$, $\chi_{AD}N = \chi_{CD}N = 60$, $\chi_{BD}N = -17$, $f_1 = 0.75$, $f_2 = 0.62$, and $\gamma = 0.16$, where HEX_B, HEX_A, and TET_A phases correspond to $\phi_2 = 0.10$, 0.68, and 0.71, respectively.

in Fig. 3. A comparison of the HEX_B and HEX_A structures indicates that the regions occupied by the A blocks undergo a transformation from a continuous matrix to discrete domains when ϕ_2 is increased. These results are consistent with experimental observations.[20]

The spatial distributions of the different blocks for the HEX_B, HEX_A, and TET_A structures are shown in Fig. 6, providing information on the compositional symmetry, domain morphology, and phase inversion behavior in the different self-assembled structures. For the HEX_B phase shown in the top panel of Fig. 6, the density maps reveal hexagonally packed circular B domains embedded within a continuous matrix composed of A and C blocks. The C and D blocks are enriched slightly at the A/B interfaces, as shown by the red rings in the C-density plot, indicating their role as co-surfactants regulating the interfacial properties. The A and C distribution confirms that the A and C blocks jointly constitute the majority matrix, while the B and D blocks form the minority domains, resulting in a conventional cylindrical structure. In contrast, the HEX_A phase shown in the middle panel of Fig. 6 exhibits a fully inverted morphology. Here, the A blocks are predominantly localized at the center of discrete circular cylinders, whereas the B and D blocks are concentrated in the interstitial regions and form a hexagonal skeleton surrounding the AC cylinders. Within the AC cylinders, the A and C blocks form a core–shell structure where the longer A blocks extend to the center of the cylinder, while the C blocks form a ring near the A/B interface. The formation of the core–shell structure provides a mechanism to stabilize large cylinders and spheres,[35,36] resulting in the morphological reversal from the conventional HEX_B structure to the inverted HEX_A phase. One interesting result from the SCFT calculations is the emergence of the inverted tetragonal (TET_A) phase. The block density maps of this novel structure, shown in the bottom panel of Fig. 6, indicate a significant anisotropic distribution of the AB and CD DBCPs in the structure. Instead of forming A/C core–shell cylinders, the density distributions of the TET_A phase indicate a separation of the A and C blocks, resulting in the formation of individual A and C domains. While the long A blocks extend to the center of the cylinders, the C blocks are localized in the regions between the A cylinders. Meanwhile, the B and D blocks form a tetragonal skeleton surrounding the A cylinders.

The distribution of different blocks in the self-assembled structures provides useful information about the mechanisms stabilizing the inverted phases. As an example, we examine the spatial arrangement of the different (A, B, C, and D) blocks in the HEX_B and HEX_A structures. Figure 7 presents two-dimensional density maps and one-dimensional density profiles of the different blocks. Specifically, two-dimensional color maps of the density fields in the x–y plane for the HEX_B and HEX_A phases are given in Figs. 7(a) and 7(e), respectively. Here, the red and blue regions denote areas where the local volume fractions satisfy $\phi_A > 0.5$ and $\phi_B + \phi_D > 0.5$, respectively, while the white regions correspond to domains dominated by A and C segments. The density plot shown in Fig. 7(a) indicates

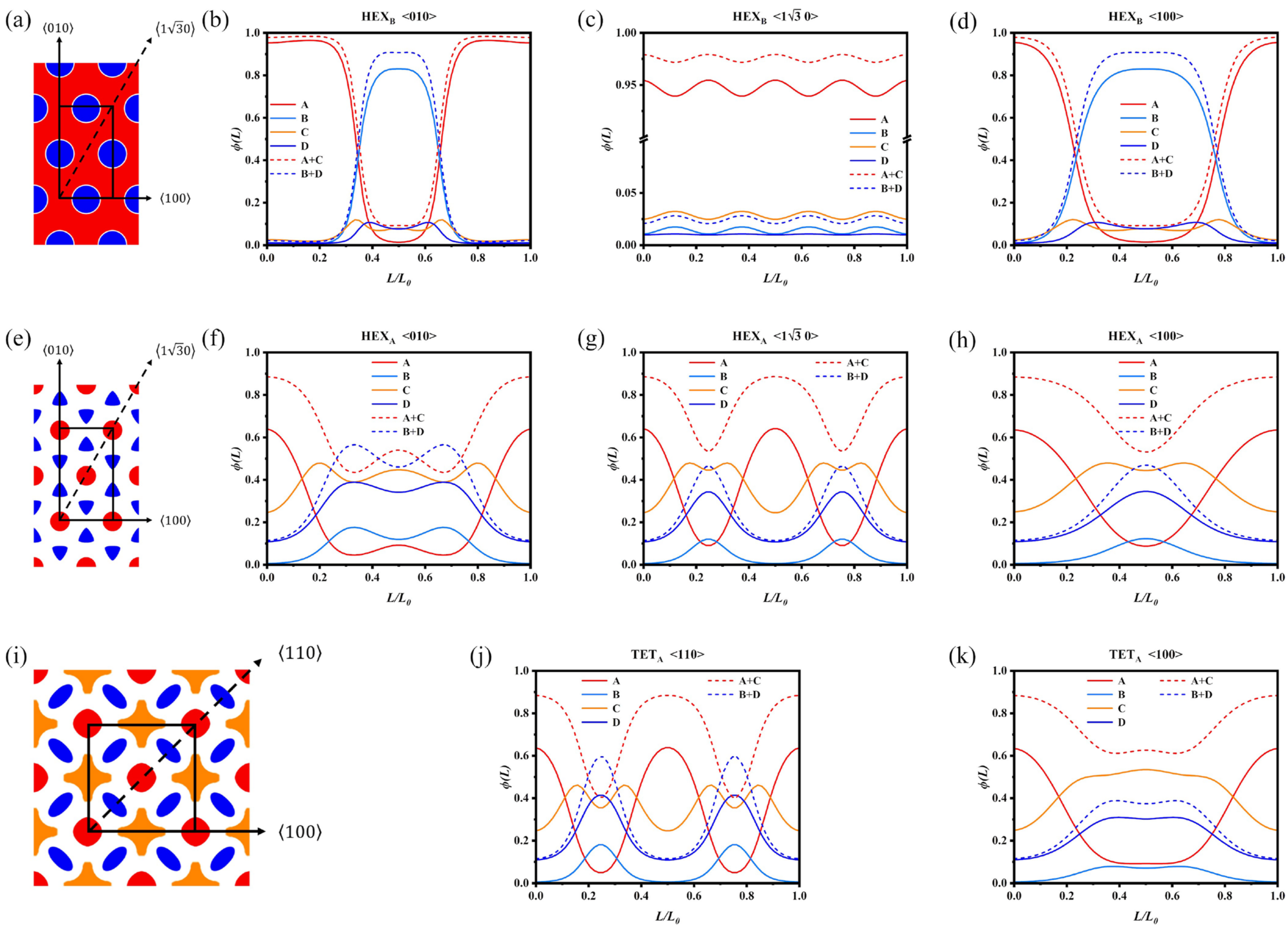

FIG. 7. Two-dimensional color maps of the segmental density distributions for three phases: (a) HEX_B with $(\chi_{BD}N, \phi_2) = (-17, 0.10)$, (e) HEX_A with $(\chi_{BD}N, \phi_2) = (-17, 0.68)$, and (i) TET_A phase with $(\chi_{BD}N, \phi_2) = (-17, 0.71)$. The red and blue regions correspond to areas with $\phi_A > 0.5$ and $\phi_B + \phi_D > 0.5$, respectively, while white regions indicate $\phi_A + \phi_C > 0.5$. The orange regions in (i) correspond to areas where the local volume fractions satisfy $\phi_C > 0.5$. (b)–(d) One-dimensional profiles of the local concentration of each component, A + C, and B + D in the HEX_B phase along the ⟨100⟩, $\langle 1\sqrt{3}0 \rangle$, and ⟨010⟩ directions. (f)–(h) Corresponding profiles for the HEX_A phase. (j)–(k) Concentration profiles for the TET_A phase along the ⟨100⟩ and ⟨110⟩ directions. The rest of the parameters are $\chi_{AB}N = \chi_{BC}N = 30$, $\chi_{AC}N = 0$, $\chi_{AD}N = \chi_{CD}N = 60$, $f_1 = 0.75$, $f_2 = 0.62$, and $\gamma = 0.16$.

that the HEX_B structure possesses a conventional cylindrical morphology dominated by the majority AB component with $\phi_1 = 0.90$, where the B-rich domains form a hexagonally packed array embedded in a continuous A matrix. To quantify the block distributions, one-dimensional density profiles of each block, as well as those of ϕ_{A+C} and ϕ_{B+D}, along three directions in the x–y plane, that is, the ⟨100⟩, $\langle 1\sqrt{3}0 \rangle$, and ⟨010⟩ directions, are shown in Figs. 7(b)–7(d) for HEX_B and Figs. 7(f)–7(h) for HEX_A, respectively. These density plots clearly indicate that the spatial arrangement of the CD DBCPs with $\phi_2 = 0.10$ exhibits qualitatively different behaviors from the AB DBCPs. Specifically, the A and B blocks form the A matrix and B cylinders, whereas the CD DBCPs are mainly distributed in the B domains with a slightly enriched segregation at the A/B interfaces. This behavior is expected due to the B/D attraction, C/D repulsion, and the length of CD DBCPs. The shorter CD diblock copolymers possess a dual function as fillers of the B domains and as co-surfactants of the A/B interfaces.[37–40]

In contrast, the density plot of the HEX_A structure [Fig. 7(e)] reveals an inverted morphology, where the A and C blocks form discrete cylindrical domains with a core–shell structure surrounded by a continuous matrix composed of B and D blocks. It is noted that the concentration of the CD DBCPs is $\phi_2 = 0.68$ in this case, so that the CD DBCPs are the majority component of the blend. The formation of well-defined AC and BD regions within the structure is clearly shown in the density profiles along the three directions (Fig. 7). Furthermore, these plots also reveal that the AC domains assume a core–shell structure where the A blocks extend to the center forming the core, whereas the C blocks form a shell near the AC and

BD interface. On the other hand, the B and D blocks are uniformly mixed, forming a continuous skeleton surrounding the AC domains. It is noted that the density of B and D blocks exhibits variations in the B + D domains, particularly shown in Fig. 7. The rich variation of the density profiles in the AC and BD domains reflects the nontrivial character of the inverted HEX_A phase. The morphological reversal from the conventional HEX_B structure to the inverted HEX_A phase could be attributed to the formation of the core–shell structure, which provides a mechanism to stabilize large cylinders and spheres.[35]

The A and C blocks can form separated domains when the concentration of the CD DBCPs is further increased and when the BD attraction is sufficiently strong. This morphological characteristic of the inverted structures is revealed in the segmental density distributions of the TET_A phase (Fig. 7). Here the two-dimensional density map in Fig. 7(i) reveals a tetragonal packing symmetry, where A-rich (red), C-rich (orange), and B + D-rich (blue) domains are periodically arranged in a tiled configuration. Compared to the HEX_A phase, the TET_A morphology exhibits enhanced anisotropy and more pronounced compositional differentiation among all four components. The corresponding one-dimensional density profiles along the ⟨100⟩ and ⟨110⟩ directions, shown in Figs. 7(j) and 7(k), offer detailed insights into the spatial organization of each segment. Along the ⟨100⟩ direction, the A and C segments display broad and separated peaks, indicating the formation of separated A and C domains in the structure. Meanwhile, the B and D segments are confined to narrow regions forming a skeleton surrounding the A and C domains. Compared with the HEX_A structure, where the A and C blocks assume a core–shell configuration, the TET_A phase represents a different chain arrangement to accommodate the large chain-length asymmetry between the two copolymers by forming separated A and C domains, thereby mitigating the packing frustration.

C. Effects of interaction strength

The results presented above demonstrate that various inverted phases can be stabilized by increasing the concentration of the shorter CD DBCPs for a given set of interaction parameters. It is natural to inquire about the effects of varying the interaction parameters. In this subsection, the effects of varying the interaction parameters on the phase behavior of the AB/CD blends are examined. There are six Flory–Huggins interaction parameters between the four different blocks, and independently varying all of these parameters presents a daunting task. To highlight the effects of the various repulsive interactions between the different blocks, we selected the following set of parameters with $\chi_{AB}N = 30$, $\chi_{AC}N = 0$, $\chi_{AD}N = 60$, $\chi_{BC}N = 30$, $\chi_{BD}N = -17.25$, $\chi_{CD}N = 60$, $f_1 = 0.75$, $f_2 = 0.62$, and $\gamma = 0.16$ as the reference system, and we investigate how the phase transition sequence is affected by varying the interaction parameters. Specifically, phase diagrams of the blends are constructed for a set of interaction parameters specified by $\chi_{AB}N = \chi_{BC}N = 30c$, $\chi_{AC}N = 0$, $\chi_{AD}N = \chi_{CD}N = 60c$, and $\chi_{BD}N = -17.25c$. This choice of scaling all the interaction strengths by a common factor c is motivated by the observation that the interaction strength between two blocks is quantified by the product $\chi_{\alpha\beta}N$, which could be adjusted by changing the degree of polymerization N or the Flory–Huggins interaction parameter $\chi_{\alpha\beta}$. Because the temperature dependence of the Flory–Huggins parameter is generally given by $\chi_{\alpha\beta} = A_{\alpha\beta}/T + B_{\alpha\beta}$, a common scaling factor c introduced here could qualitatively describe the effect of varying the overall degree of polymerization N and the temperature T if $B_{\alpha\beta}$ is small.

The effect of varying the common scaling factor c on the phase behavior of the AB/CD blends is displayed in the phase diagrams shown in Figs. 8(a) and 8(b). When the value of c is increased from 0.5 to 2.0, the neat AB DBCP melt exhibits a phase transition sequence of Dis → BCC_B → HEX_B, whereas the neat CD diblock copolymer melt exhibits a different phase transition sequence of Dis → BCC_D → HEX_D → DG_D → L. It is interesting to note that, as c is varied, a rich phase behavior with various new ordered phases is

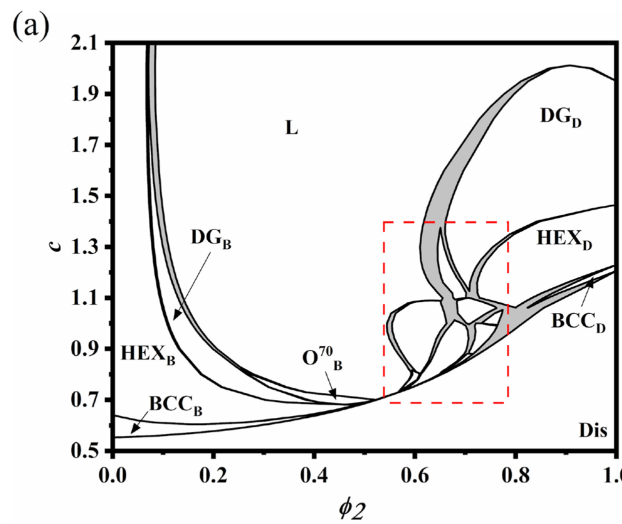

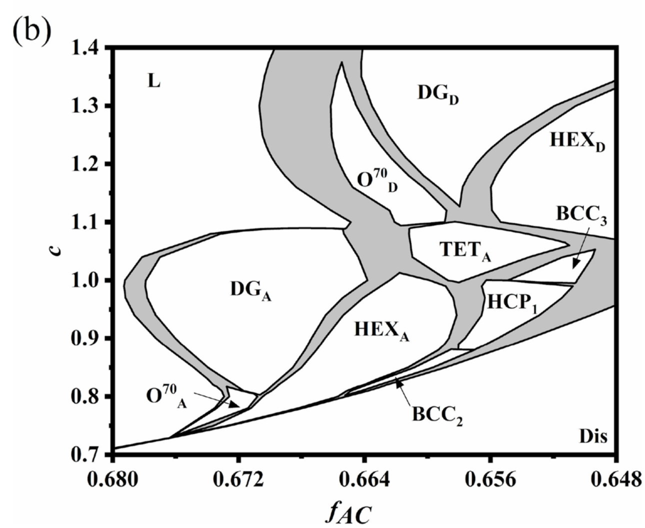

FIG. 8. Phase diagrams of AB/CD DBCP blends under different scaling and repulsion conditions with $\chi_{AB}N = \chi_{BC}N = 30c$, $\chi_{AC}N = 0$, $\chi_{AD}N = \chi_{CD}N = 60c$, $\chi_{BD}N = -17.25c$, $f_1 = 0.75$, $f_2 = 0.62$, and $\gamma = 0.16$: (a) c–ϕ_2 plane and (b) c–f_{AC} plane corresponding to the inverted-phase region highlighted by the red dashed box in (a).

observed in the AB/CD blends, as shown in Fig. 8(a). In particular, several inverted phases are stabilized within the region $0.53 < \phi_2 < 0.80$ and $0.7 < c < 1.1$, as shown by the red box in Fig. 8(a) and in the $c - f_{AC}$ plane in Fig. 8(b). When the value of c is changed from 0.5 to 2.0, several interesting phase transition sequences, such as Dis→ O^{70}_A → DG_A →L and Dis→ BCC_2 → HEX_A → TET_A → O^{70}_D → DG_D, are predicted for the AB/CD blends.

D. Effects of chain length and block composition

It is expected that varying the chain length and/or block composition will affect the phase behavior of the AB/CD blends. In order to elucidate the structural transition and the emergence of inverted morphologies, we focus on the influence of two key parameters: the ratio of polymerization degrees γ and the block composition f_2 of the CD DBCPs. In particular, the value of $\gamma = 0.16$ in our system corresponds to weak segregation between the A/C and D domains, which allows for partial mixing and enables curvature adaptation. Meanwhile, increasing f_{AC} effectively enriches the A and C components, thereby enhancing packing frustration and promoting phase inversion. This compositional bias and interfacial modulation create favorable conditions for the stabilization of HEX_A and TET_A phases. As previously noted, attractive interactions between blocks B and D are not a strict prerequisite for forming inverted phases. Instead, the chain length ratio γ emerges as a critical factor. Using the same parameters as before ($\chi_{AB}N = 30$, $\chi_{AC}N = 0$, $\chi_{AD}N = 60$, $\chi_{BC}N = 30$, $\chi_{BD}N = -17.25$, $\chi_{CD}N = 60$, $f_1 = 0.75$, $f_2 = 0.62$), the γ–ϕ_2 phase diagram shown in Fig. 9(a) confirms that inverted phases only appear when $\gamma < 0.18$. Moreover, the inverted phase regime in the $\gamma - f_{AC}$ plane is shown in Fig. 9(b), which further shows that $A15_A$ and σ_A morphologies become stable at $\gamma < 0.15$, highlighting the crucial role of chain length asymmetry in stabilizing such complex structures.

In addition to the ratio of BCP chain lengths γ, the C-volume fraction f_2 of the CD DBCPs significantly influences the phase behavior of the AB/CD blends. Figure 9(c) presents the $f_2 - \phi_2$ phase diagram at fixed $\gamma = 0.16$, showing that inverted phases are stabilized

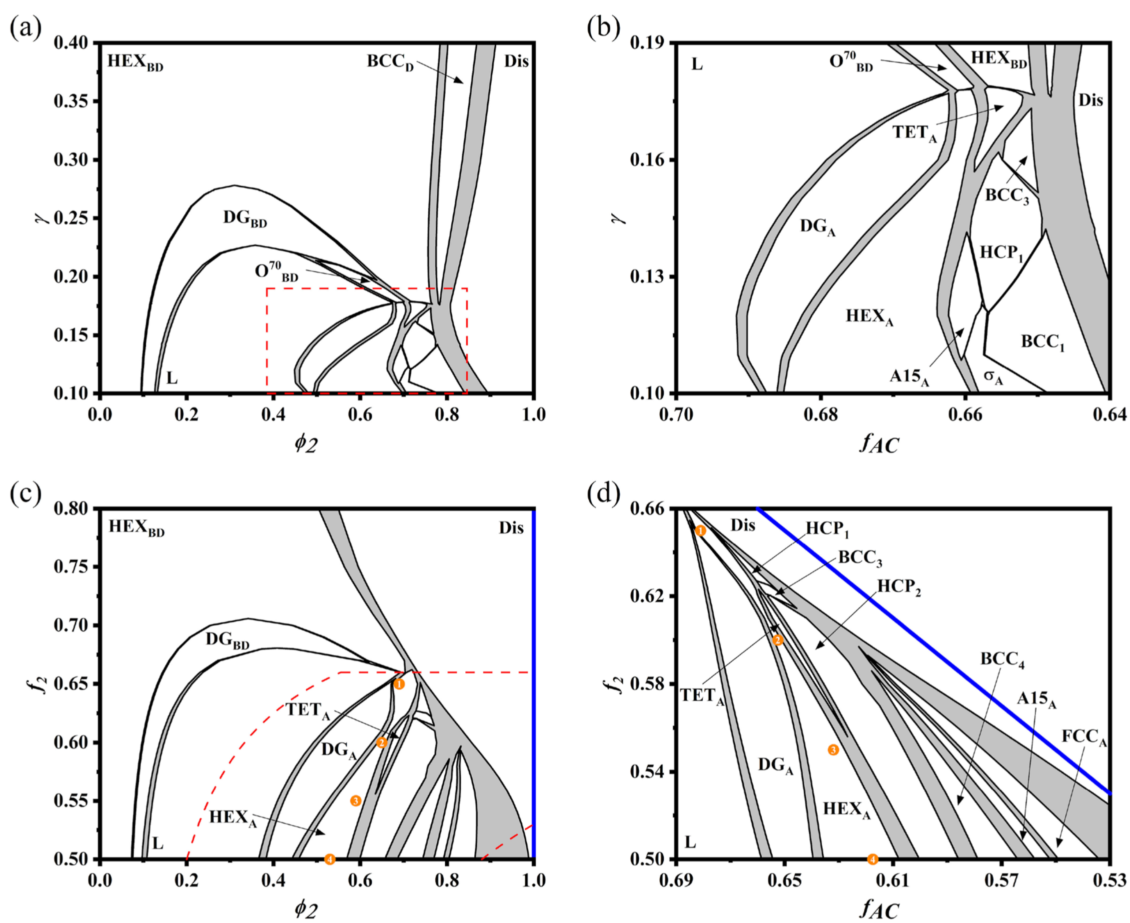

FIG. 9. Phase diagrams highlighting the effects of polymerization asymmetry and blend composition on phase behavior in AB/CD diblock copolymer systems with $\chi_{AB}N = \chi_{BC}N = 30$, $\chi_{AC}N = 0$, $\chi_{AD}N = \chi_{CD}N = 60$, $\chi_{BD}N = -17.25$, $f_1 = 0.75$: (a) γ–ϕ_2 plane with $f_2 = 0.62$; (b) γ–f_{AC} plane corresponding to the inverted-phase region highlighted by the red dashed box in (a); (c) f_2–ϕ_2 plane with $\gamma = 0.16$; (d) f_2–f_{AC} plane corresponding to the inverted-phase region highlighted by the red dashed box in (c). The blue lines in (c) and (d) mark the same phase path. The numbered orange dots in (c) and (d) indicate points inside the HEX_A region along a path with increasing f_{AC}.

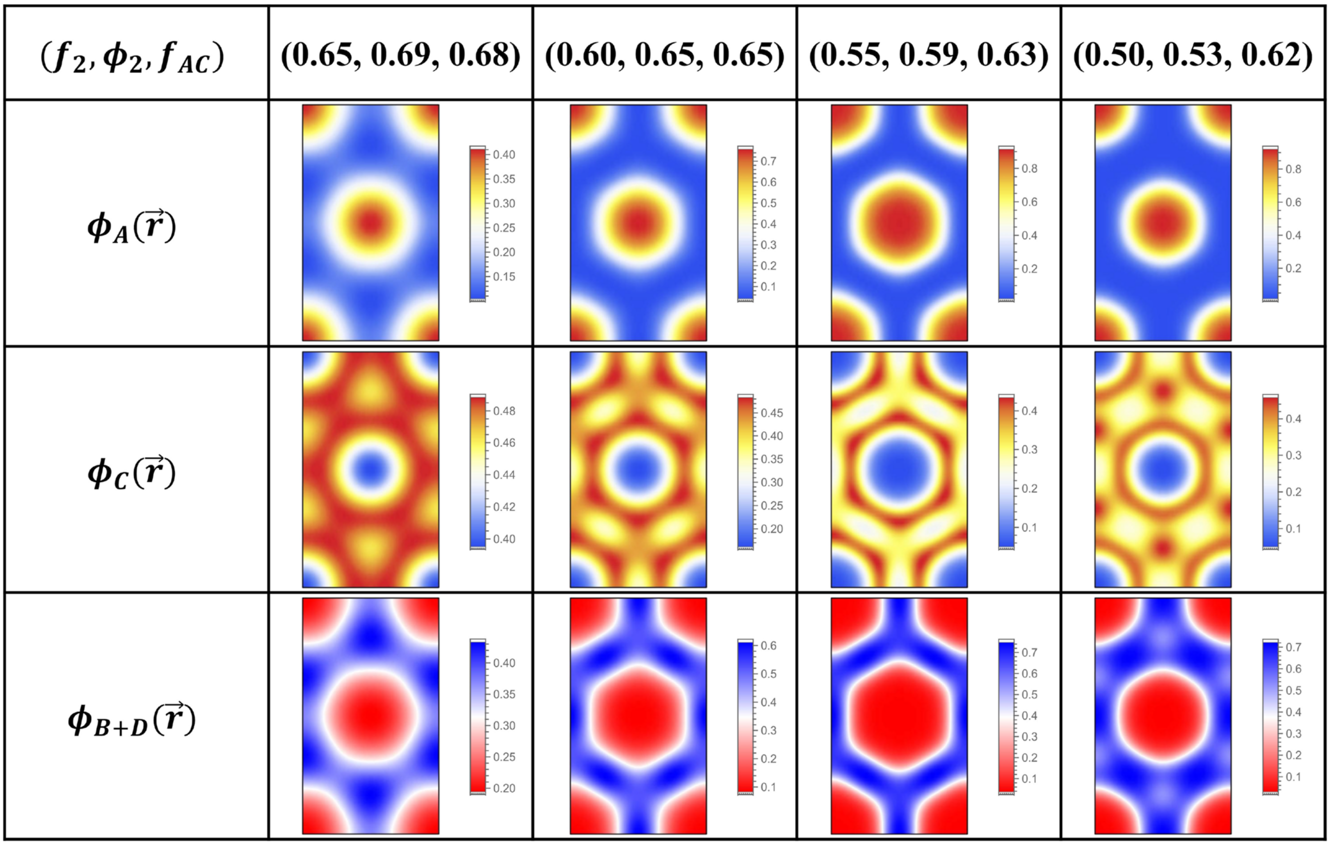

FIG. 10. Color map of the spatial distributions of the A, C, and B + D components in HEX_A structure for different values of f_2 and ϕ_2, (f_2, ϕ_2, f_{AC})=(0.65, 0.69, 0.68), (0.60, 0.65, 0.65), (0.55, 0.59, 0.63), and (0.50, 0.53, 0.62), corresponding to the orange points 1, 2, 3, and 4 shown in Figs. 9(c) and 9(d).

only when $f_2 < 0.66$. Notably, the TET_A phase appears in a narrow channel within the $0.56 < f_2 < 0.62$ range, while other inverted morphologies such as BCC_4 and FCC_A are also observed at $f_2 < 0.6$. As shown in Fig. 9(d), the range of f_{AC} increases with decreasing f_2, and the shift in morphology is visually illustrated in Fig. 10, where the spatial distribution of A, C and BD components in the HEX_A structures at the four points indicated by the orange dots in Figs. 9(c) and 9(d) are displayed. These points on the phase diagram are selected in the region where the HEX_A phase is stable. It is found that the BD domains in the HEX_A structures gradually evolve from being concentrated near the interstitial voids at point 1 ($f_2 = 0.65$, $\phi_2 = 0.69$) to becoming slightly depleted in these regions at point 4 ($f_2 = 0.50$, $\phi_2 = 0.53$). The distributions of the A and C blocks reveal a core–shell structure composed of an A core and a C shell. The relationship between the dimensions of the core–shell structure and the block copolymer parameters, and the variation of the shell structure, are also seen in the density profiles of the A and C blocks shown in Fig. 10. Qualitatively, the shell thickness decreases with decreasing f_{AC}. At smaller f_2 and ϕ_2 values, particularly at point 4, the depletion of the BD blocks from the interstitial regions is accompanied by the emergence of clear density peaks of the C blocks in these regions. This progression reflects a fundamental shift in the role of the CD copolymers: at higher f_2, they act as interfacial co-surfactants that stabilize curvature between segregated A and B domains; as f_2 decreases, the CD chains instead function as structural fillers within the minority BD matrix, helping to restore matrix connectivity and reduce packing frustration. Therefore, the range $f_2 < 0.66$ appears optimal for achieving robust inverted phases while maintaining sufficient curvature adaptability at the interface, and the critical condition to form inverted phases is that a sufficient amount of the short CD copolymers acts as spatial fillers without compromising too much interfacial energy.

IV. CONCLUSION

In this study, we employed the self-consistent field theory (SCFT) to investigate the formation of inverted phases in binary blends of linear AB and CD diblock copolymers. Our results reveal that several inverted morphologies—including HEX_A and TET_A—are stabilized only within specific parameter spaces, most notably when the polymerization degree ratio satisfies $\gamma < 0.18$ and the volume fraction of the C-block in the CD copolymer lies within $0.50 < f_2 < 0.66$. These conditions correspond to a compositional and geometric asymmetry that promotes the formation of curvature-inverted structures. A central finding of this work is the identification of the role played by the CD diblock copolymers. At higher f_2, CD chains act as co-surfactants localized at the A/B interface, reducing interfacial tension and facilitating domain curvature. In contrast, at lower f_2, CD copolymers behave as structural fillers that reinforce the BD matrix and suppress connectivity loss in the minority phase. This shift in function is closely related to the mechanism of inversion, which balances enthalpic segregation, chain stretching penalties, and interfacial curvature adaptation. These results underscore the broader strategy of using block copolymer blends to regulate self-assembly pathways and access morphologies that are inaccessible to neat systems. By tuning molecular composition and interaction asymmetry, complex structures such as inverted phases can be stabilized.

Our results are consistent with experimental observations of inverted morphologies in triblock copolymers and block copolymer blends mentioned in the review by Woo *et al.*,[7] especially under conditions of molecular asymmetry and selective attraction. The phase diagrams and real-space morphologies obtained here offer mechanistic insights into these experimental systems and support the broader strategy of using BCP blending to modulate domain structure and curvature. Beyond theoretical interest, these findings provide practical guidelines for designing nanostructured materials with tunable topology and connectivity. The controlled emergence of inverted phases offers pathways for fabricating templates for nanolithography, high-surface-area membranes, and photonic materials. Future extensions of the current work include studies incorporating conformational asymmetry, dispersity, or external field effects, thereby broadening the design space for functionally complex polymer-based nanostructures.

ACKNOWLEDGMENTS

This research was supported by the Natural Sciences and Engineering Research Council (NSERC) of Canada and was enabled in part by support provided by the facilities of SHARCNET (https://www.sharcnet.ca) and the Digital Research Alliance of Canada (alliancecan.ca).

AUTHOR DECLARATIONS

Conflict of Interest

The authors have no conflicts to disclose.

Author Contributions

Yuhui Yi: Conceptualization (equal); Data curation (lead); Formal analysis (equal); Methodology (equal); Writing – original draft (equal); Writing – review & editing (equal). **Jiayu Xie**: Conceptualization (equal); Formal analysis (equal); Methodology (equal); Writing – review & editing (equal). **Jiajia Zhou**: Conceptualization (equal); Formal analysis (equal); Funding acquisition (equal); Writing – review & editing (equal). **An-Chang Shi**: Conceptualization (lead); Formal analysis (equal); Funding acquisition (lead); Methodology (equal); Supervision (lead); Writing – original draft (equal); Writing – review & editing (equal).

DATA AVAILABILITY

The data that support the findings of this study are available from the corresponding author upon reasonable request.

REFERENCES

[1] C. M. Bates and F. S. Bates, "50th anniversary perspective: Block polymers—Pure potential," Macromolecules **50**, 3–22 (2017).
[2] F. S. Bates and G. H. Fredrickson, "Block copolymers—Designer soft materials," Phys. Today **52**(2), 32–38 (1999).
[3] N. Xie, W. Li, F. Qiu, and A.-C. Shi, "σ phase formed in conformationally asymmetric AB-Type block copolymers," ACS Macro Lett. **3**, 906–910 (2014).
[4] M. W. Schulze, R. M. Lewis III, J. H. Lettow, R. J. Hickey, T. M. Gillard, M. A. Hillmyer, and F. S. Bates, "Conformational asymmetry and quasicrystal approximants in linear diblock copolymers," Phys. Rev. Lett. **118**, 207801 (2017).
[5] A.-C. Shi, "Frustration in block copolymer assemblies," J. Phys.: Condens. Matter **33**, 253001 (2021).
[6] M. W. Matsen, "The standard Gaussian model for block copolymer melts," J. Phys.: Condens. Matter **14**, R21 (2001).
[7] D. Woo, H. Yoon, and J. K. Kim, "Unconventional microdomains of block copolymers," J. Polym. Sci. **62**, 639–661 (2024).
[8] B. H. Kim, J. Y. Kim, and S. O. Kim, "Directed self-assembly of block copolymers for universal nanopatterning," Soft Matter **9**, 2780–2786 (2013).
[9] J. A. Dolan, B. D. Wilts, S. Vignolini, J. J. Baumberg, U. Steiner, and T. D. Wilkinson, "Optical properties of gyroid structured materials: From photonic crystals to metamaterials," Adv. Opt. Mater. **3**, 12–32 (2015).
[10] W. A. Phillip, B. O'Neill, M. Rodwogin, M. A. Hillmyer, and E. L. Cussler, "Self-assembled block copolymer thin films as water filtration membranes," ACS Appl. Mater. Interfaces **2**, 847–853 (2010).
[11] E. R. Pico and M. C. Williams, ""Thermodynamics of plasticized triblock copolymers. I. Theory," J. Polym. Sci.: Polym. Phys. Ed. **15**, 1585–1600 (1977).
[12] E. R. Pico and M. C. Williams, "Thermodynamics of plasticized triblock copolymers. Part II: Model verification by light transmittance and rheology," Polym. Eng. Sci. **17**, 573–581 (1977).
[13] L. Yang, S. Hong, S. P. Gido, G. Velis, and N. Hadjichristidis, "I_5S Miktoarm star block copolymers: Packing constraints on morphology and discontinuous Chevron tilt grain boundaries," Macromolecules **34**, 9069–9073 (2001).
[14] G. Liontos, G.-M. Manesi, I. Moutsios, D. Moschovas, A. A. Piryazev, E. A. Bersenev, D. A. Ivanov, and A. Avgeropoulos, "Synthesis, molecular characterization, and phase behavior of Miktoarm star copolymers of the AB_n and A_nB (n= 2 or 3) sequences, where A is polystyrene and B is poly(dimethylsiloxane)," Macromolecules **55**, 88–99 (2021).
[15] Y. Seo, D. Woo, L. Li, W. Li, and J. K. Kim, "Phase behavior of PS-(PS-b-P2VP)$_3$ miktoarm star copolymer," Macromolecules **54**, 7822–7829 (2021).
[16] Q. Zhang, O. K. C. Tsui, B. Du, F. Zhang, T. Tang, and T. He, "Observation of inverted phases in poly(styrene-*b*-butadiene-*b*-styrene) triblock copolymer by solvent-induced order−disorder phase transition," Macromolecules **33**, 9561–9567 (2000).
[17] J. Xie and A.-C. Shi, "Phase behavior of binary blends of diblock copolymers: Progress and opportunities," Langmuir **39**, 11491–11509 (2023).
[18] D. Yamaguchi, H. Hasegawa, and T. Hashimoto, "A phase diagram for the binary blends of nearly symmetric diblock copolymers. 2. Parameter space of temperature and blend composition," Macromolecules **34**, 6506–6518 (2001).
[19] S. Kang, J. Lee, E. Kim, Y. Seo, C. Choi, and J. K. Kim, "Inverted cylindrical microdomains from binary block copolymer blends capable of hydrogen bonding," Macromolecules **54**, 8971–8976 (2021).
[20] S. Kang, J. Lee, H. Yoon, J. Jang, E. Kim, and J. K. Kim, "Tetragonally packed inverted cylindrical microdomains from binary block copolymer blends with enhanced hydrogen bonding," ACS Macro Lett. **12**, 915–920 (2023).
[21] Q. Li, D. Woo, J.-K. Kim, and W. Li, "Truly 'inverted' cylinders and spheres formed in the A(AB)$_3$/AC blends of B/C hydrogen bonding interactions," Macromolecules **55**, 6525–6535 (2022).
[22] J. Xie, C. T. Lai, and A.-C. Shi, "Regulating the self-assembly of AB/CD diblock copolymer blends via secondary interactions," J. Polym. Sci. **62**, 716–732 (2024).

[23] B. R. Magruder, S. J. Park, R. P. Collanton, F. S. Bates, and K. D. Dorfman, "Laves phase field in a diblock copolymer alloy," Macromolecules **55**, 2991–2998 (2022).
[24] L. J. Case, F. S. Bates, and K. D. Dorfman, "Tuning conformational asymmetry in particle-forming diblock copolymer alloys," Soft Matter **19**, 90–97 (2023).
[25] A. Dehghan and A.-C. Shi, "Modeling hydrogen bonding in diblock copolymer/homopolymer blends," Macromolecules **46**, 5796–5805 (2013).
[26] G. Fredrickson, *The Equilibrium Theory of Inhomogeneous Polymers* (Oxford University Press, 2005), Vol. 134.
[27] A.-C. Shi, "Self-consistent field theory of inhomogeneous polymeric systems," in *Variational Methods in Molecular Modeling*, edited by J. Wu (Springer, 2016).
[28] W. Li and A.-C. Shi, "Self-consistent field theory of self-assembling multiblock copolymers," in *Self-Assembling Systems: Theory and Simulation*, edited by L.-T. Yan (Wiley, 2017).
[29] W. Xu, K. Jiang, P. Zhang, and A.-C. Shi, "A strategy to explore stable and metastable ordered phases of block copolymers," J. Phys. Chem. B **117**, 5296–5305 (2013).
[30] K. Ø. Rasmussen and G. Kalosakas, "Improved numerical algorithm for exploring block copolymer mesophases," J. Polym. Sci., Part B: Polym. Phys. **40**, 1777–1783 (2002).
[31] G. Tzeremes, K. Ø. Rasmussen, T. Lookman, and A. Saxena, "Efficient computation of the structural phase behavior of block copolymers," Phys. Rev. E **65**, 041806 (2002).
[32] R. B. Thompson, K. O. Rasmussen, and T. Lookman, "Improved convergence in block copolymer self-consistent field theory by Anderson mixing," J. Chem. Phys. **120**, 31–34 (2004).
[33] A. Arora, D. C. Morse, F. S. Bates, and K. D. Dorfman, "Accelerating self-consistent field theory of block polymers in a variable unit cell," J. Chem. Phys. **146**, 244902 (2017).
[34] J. Kwak, S. H. Han, H. C. Moon, J. K. Kim, V. Pryamitsyn, and V. Ganesan, "Effect of the degree of hydrogen bonding on asymmetric lamellar microdomains in binary block copolymer blends," Macromolecules **48**, 6347–6352 (2015).
[35] W. Li, C. Duan, and A.-C. Shi, "Nonclassical spherical packing phases self-assembled from AB-type block copolymers," ACS Macro Lett. **6**, 1257–1262 (2017).
[36] J. Xie, Y. Li, and A.-C. Shi, "Binary blends of diblock copolymers: An efficient route to complex spherical packing phases," Macromol. Theory Simul. **30**, 2100053 (2021).
[37] S. Lee, M. J. Bluemle, and F. S. Bates, "Discovery of a Frank-Kasper σ phase in sphere-forming block copolymer melts," Science **330**, 349–353 (2010).
[38] K. D. Dorfman, "Frank–Kasper phases in block polymers," Macromolecules **54**, 10251–10270 (2021).
[39] M. Matsuo, S. Sagae, and H. Asai, "Fine structures of styrene-butadiene block copolymer films cast from toluene solution," Polymer **10**, 79–87 (1969).
[40] M. W. Matsen, "Effect of architecture on the phase behavior of AB-type block copolymer melts," Macromolecules **45**, 2161–2165 (2012).